Hindawi
Complexity
Volume 2019, Article ID 6083853, 15 pages
https://doi.org/10.1155/2019/6083853

Research Article

Dynamic Behaviors Analysis of a Chaotic Circuit Based on a Novel Fractional-Order Generalized Memristor

Ningning Yang,[1,2] **Shucan Cheng**,[2] **Chaojun Wu**,[3] **Rong Jia**,[1,2] **and Chongxin Liu**[4]

[1] *State Key Laboratory Base of Eco-Hydraulic Engineering in Arid Area, Xi'an University of Technology, Xi'an 710048, China*
[2] *Institute of Water Resources and Hydroelectric Engineering, Xi'an University of Technology, Xi'an 710048, China*
[3] *College of Electronics and Information, Xi'an Polytechnic University, Xi'an 710048, China*
[4] *School of Electrical Engineering, Xi'an Jiaotong University, Xi'an 710049, China*

Correspondence should be addressed to Shucan Cheng; shucanc@stu.xaut.edu.cn and Chaojun Wu; chaojun.wu@stu.xjtu.edu.cn

Received 29 January 2019; Revised 31 March 2019; Accepted 5 May 2019; Published 21 May 2019

Academic Editor: Honglei Xu

In this paper, a fractional-order chaotic circuit based on a novel fractional-order generalized memristor is proposed. It is proved that the circuit based on the diode bridge cascaded with fractional-order inductor has volt-ampere characteristics of pinched hysteresis loop. Then the mathematical model of the fractional-order memristor chaotic circuit is obtained. The impact of the order and system parameters on the dynamic behaviors of the chaotic circuit is studied by phase trajectory, Poincaré Section, and bifurcation diagram method. The order, as an important parameter, can increase the degree of freedom of the system. With the change of the order and parameters, the circuit will exhibit abundant dynamic behaviors such as coexisting upper and lower limit cycle, single scroll chaotic attractors, and double scroll chaotic attractors under different initial conditions. And the system exhibits antimonotonic behavior of antiperiodic bifurcation with the change of system parameters. The equivalent circuit simulations are designed to verify the results of the theoretical analysis and numerical simulation.

1. Introduction

The memristor, which is considered as the fourth basic circuit element, was first proposed theoretically by Professor Leon Chua in 1971[1]. Since the development of the practical memristor in HP Laboratory in 2008 [2], the practical application of memristors has attracted wide attention. At present, the research on the memristor mainly focuses on its physical realization such as memristor equivalent circuits [3–5], the dynamical behaviors of chaotic circuits based on the memristor [6–9], and memristive neural networks [10, 11]. As a basic circuit element, memristor is mostly used in various fields in the form of circuit at present, so the application circuit of memristor is rich and diverse. Because memristor has natural nonlinearity and plasticity, it is easy to construct chaotic oscillation circuit based on memristor by organic combination with other circuit elements.

If the volt-ampere characteristics of the circuit ports have three characteristics fingerprints as described in [12], it can be defined as a memristor. Reference [3] presents a generalized memristor diode bridge circuit of cascaded RLC filters consisting of full-wave rectifiers and second-order RLC filters. Reference [4] presents a generalized memristor simulator for first-order parallel RC filters cascaded by a diode bridge. In [5], a first-order generalized memristor simulator based on diode bridge and series RL filter is proposed. In [13], a fractional-order generalized memristor consisting of a diode bridge and a parallel circuit with an equivalent unit circuit and a linear resistance is proposed. If only an inductor cascades a diode bridge, the circuit has simpler topology while it satisfies the memristor characteristics. All the generalized memristor can be simplified as a nonlinear basic element.

The concept of fractional calculus is a development in the field of mathematics, which can be applied to describe memristor characteristics. Fractional calculus plays an important role in signal and image processing [14, 15], control theory [16], and nonlinear dynamical systems [17–21]. A large number of studies have shown that the introduction of fractional-order parameters as adjustable parameters in the

model improves the degree of freedom of the model and can more accurately describe the characteristics of actual systems. Because magnetic flux or charge is mathematically a time integral of voltage or current, it can show itself a memory feature [22]. Fractional calculus is especially suitable for describing the memory and hereditary characteristics of the system [23, 24]. It has essentially the same mathematical principles as the memory characteristics of memory circuit elements. It is feasible to introduce fractional calculus theory into the dynamic behavior analysis and application of memory circuit elements [25, 26]. The relationship between fractional calculus and the behavior of memory system is proposed in [17], and it is pointed out that the memristor can be extended to fractional-order one. Reference [18] describes a classical Chua's oscillator based on fractional-order memristor, in which the memristor is a flux-controlled memristor. A novel fractional-order system consisting of memristor, capacitor, and inductor is studied in [19]. In [27], a memory resistor with noncontact polynomial memory resistance function is used in the simplest chaotic circuit. In addition, a Lorenz system based on fractional-order memristors is proposed in [21], its flux-controlled memristors have different permeance functions, and their dynamic characteristics are analyzed, respectively. However few papers mentioned that the chaotic circuit based on fractional-order memristor has coexisting period and chaotic states under different initial values and has antimonotonic behavior of antiperiodic bifurcation.

The rest of this paper mainly includes the following five sections. In Section 2, the generalized fractional-order memristor (FOM) based on single fractional-order inductor and diode bridge is proposed and its memristive characteristics are verified. Then a FOM-based fractional-order chaotic circuit is proposed consisting of a fractional-order capacitor, a fractional-order inductor, and a negative resistor. The equilibrium and stability of the circuit are analyzed. In Section 3, the dynamic behavior of the fractional-order system is analyzed. Firstly, the bifurcation diagram of the system with the order parameter is studied, and the changing process of the dynamic behavior is analyzed combined with the system trajectory under different initial conditions. Then the bifurcation diagrams of the system varying with one of the system parameters at different orders are studied. At the same time, it is found that the fractional-order system has antimonotonic behavior of coexistence and antiperiodicity under different initial conditions. In Section 4 the chaotic circuit composed of equivalent fractional-order inductor and capacitor is simulated to verify the dynamic behavior of the fractional-order chaotic circuit. The last part is the conclusion.

2. Fractional-Order Chaotic Circuit Based on Generalized Memristor

Fractional calculus can be regarded as an extension of classical integer-order calculus, but it has its own unique logic and grammar rules. There are several different definitions involving the fractional versions of the integral and derivative operators: Riemann-Liouville (RL) definition, Grunwald-Letnikov (GL) definition, and Caputo definition [23].

Because the definition of Caputo allows integer-order initial conditions to be used to solve fractional-order differential equations, it is widely used in the modeling of practical problems.

The definition of Caputo is

$$ {}_{a}^{C}\mathrm{D}_{t}^{\alpha} f(t) = \frac{1}{\Gamma(n-\alpha)} \frac{\mathrm{d}^{n}}{\mathrm{d}t^{n}} \int_{0}^{t} \frac{f(\tau)}{(t-\tau)^{\alpha-n+1}} \mathrm{d}\tau \tag{1} $$

where $n \in N$ is the first integer which is not less than α. $f(t)$ is a fractional-order derivative of a continuous function of time, which is given in terms of a time integral.

Laplace transform is a common tool for describing fractional-order systems. The integer-order Laplace transform can be generalized to the fractional-order form.

$$ L\left\{\frac{\mathrm{d}^{\alpha} x(t)}{\mathrm{d}t^{\alpha}}\right\} = s^{n} F(s) - \sum_{k=0}^{m-1} s^{k} \left[\frac{\mathrm{d}^{\alpha-(1+k)} x(t)}{\mathrm{d}t^{\alpha-(1+k)}}\right] \tag{2} $$

where m is an integer value; when the initial value of the system is zero, formula (2) can be simplified as

$$ L\left\{\frac{\mathrm{d}^{\alpha} x(t)}{\mathrm{d}t^{\alpha}}\right\} = s^{\alpha} F(s) \tag{3} $$

When $t = 0$, for single-input single-output (SISO) systems, the relationship between the input and output signals $x(t)$ and $y(t)$ is

$$ G(s) = \frac{Y(s)}{F(s)} = \frac{a_{m} s^{\beta_{m}} + a_{m-1} s^{\beta_{m-1}} + \cdots + a_{0} s^{\beta_{0}}}{b_{m} s^{\alpha_{n}} + b_{m-1} s^{\alpha_{n-1}} + \cdots + b_{0} s^{\alpha_{0}}} \tag{4} $$

where $(a_m, b_m) \in R(\forall n, m \in N)$.

2.1. Fractional-Order Memristor Based on Diode Bridge Cascaded with a Single Fractional-Order Inductor. A generalized memristor consisting of a single ideal inductor and diode bridge is proposed in [6]. Lots of researches have shown that the real capacitor and inductor can be extended to fractional-order forms to describe their real electricity characteristics. In this paper, the integer-order inductor L in the generalized memristor is extended to the fractional-order form. Then the model of integer-order memristor can be extended to the fractional-order one as shown in Figure 1.

The relation between the voltage across and the current through diodes D_k, named as v_k and i_k, respectively ($k = \{1, 2, 3, 4\}$), is modeled as

$$ i_{k} = I_{S}\left(e^{2\rho v_{k}} - 1\right) \tag{5} $$

where I_S is the reverse saturation current of the diode, $\rho = 1/(2nV_T)$, n is the emission coefficient, V_T refers to the thermal voltage, and three diode parameters are 5.84nA, 1.94, and 25mV, respectively. q stands for the order; the fractional-order mathematical model of the circuit shown in Figure 1 is

$$ i_{g} = \left(i_{L_{m}} + 2I_{S}\right) \tanh\left(\rho v_{g}\right) \tag{6} $$

$$ \frac{\mathrm{d}^{q} i_{L_{m}}}{\mathrm{d}t^{q}} = \frac{\left\{\ln\left[2I_{S}\cosh\left(\rho v_{g}\right)\right] - \ln\left(i_{L_{m}} + 2I_{S}\right)\right\}}{\left(\rho L_{m}^{q}\right)} \tag{7} $$

Table 1: Linear transfer function approximations of fractional-order integrator with order q.

q	$F(s)$
0.99	$\dfrac{s^5 + 9.87e4s^4 + 9.647e7s^3 + 9.43e8s^2 + 9.2e7s + 8.9e4}{891.3s^5 + 9.21e5s^4 + 9.43e6s^3 + 9.65e5s^2 + 987.1s + 0.01}$
0.93	$\dfrac{s^5 + 8.6e4s^4 + 7.32e7s^3 + 6.23e8s^2 + 5.3e7s + 4.47e4}{446.7s^5 + 5.3e5s^4 + 6.23e6^3 + 7.32e5s^2 + 859.7s + 0.01}$
0.9	$\dfrac{s^5 + 8.02e4s^4 + 6.37e7s^3 + 5.06e8s^2 + 4.02e7s + 3.2e4}{316.2s^5 + 4.02e5s^4 + 5.06e6^3 + 6.37e5s^2 + 802.4s + 0.01}$
0.8	$\dfrac{s^5 + 6.37e4s^4 + 4.02e7s^3 + 2.54e8s^2 + 1.6e7s + 1e4}{100s^5 + 1.6e5s^4 + 2.54e6s^3 + 4.02e5s^2 + 637.3s + 0.01}$

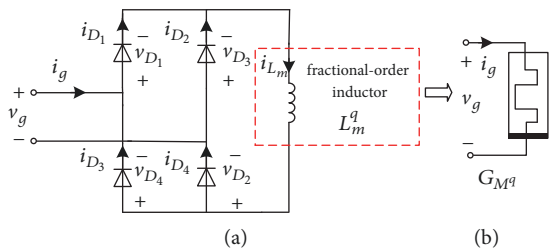

Figure 1: Model of a generalized fractional-order memristor based on diode bridge cascaded with a single fractional-order inductor.

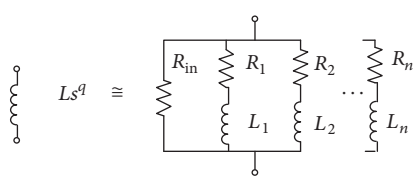

Figure 2: Equivalent unit circuit of the fractional-order inductor.

i_{L_m} refers to the current passing through the fractional-order inductor, v_g stands for the input voltage, and i_g is the input current. L_m^q is set to 10mH. This is a current-controlled FOM model. And the memconductance is

$$G_{M^q} = \frac{i_g}{v_g} = \left(i_{L_m} + 2I_S\right)\tanh\frac{\left(\rho v_g\right)}{v_g} \tag{8}$$

The fractional-order inductor is realized by equivalent unit circuit shown in Figure 2.

The electronic circuit shown in Figure 2 is constructed to implement the approximate transfer functions of fractional-order integrator operator depicted in Table 1.

The equivalent circuit expression of the fractional-order inductor is

$$\frac{1}{L}s^{-q} = \sum_{k=1}^{n}\frac{1/L_k}{s + R_k/L_k} + \frac{1}{R_{\text{in}}} \tag{9}$$

Using Oustaloup approximation method, the series number of resistors and inductors connected in parallel is $n = 2N + 1$, N is the order of the filter. Table 1 gives the approximate transfer functions of fractional-order integrator $F(s)$ when q is selected as 0.99, 0.93, 0.9, and 0.8. The corresponding values of the inductor are calculated in Table 2.

To calculate the approximate transfer functions $F(s)$, the bode diagrams of Oustaloup approximation when $q = 0.99$ and $q = 0.9$ are exhibited in Figure 3.

Four diodes 1N4148 and a voltage source $v_g = A\sin(2\pi ft)$ are selected in the Pspice circuit simulation experiment, where A and f are the amplitude and frequency of the voltage source, respectively, and the equivalent circuit model of the fractional-order inductor is built. When A is 3V and f is 100Hz, 500Hz, and 1 kHz, respectively, the volt-ampere relationship of the input port is shown in Figure 4.

It can be seen that the trajectory is a pinched hysteresis loop. With the same order, the higher the frequency, the smaller the area enclosed by the hysteresis loop. At the same frequency, when the order decreases, the maximum current of the input port increases.

In order to compare the influence of the order on the characteristics of the memristor model, the volt-ampere relationship under different order is obtained as shown in Figure 5.

The volt-ampere characteristics of the FOM model obtained in this section conform to the definition of generalized memristor. When $f = 500$Hz, as q decreases, the maximum current of the input port increases and the area of the hysteresis loop increases.

2.2. The Fractional-Order Chaotic Circuit Based on FOM. The structure of memristive chaotic circuit, which is a integer-order system, is proposed in [7]. In this paper, the inductor, capacitor, and memristor are extended to fractional order, and then the FOM-based fractional-order chaotic circuit is obtained. The structure of the FOM-based fractional-order chaotic circuit is shown in Figure 6. In addition the case of symmetry order is studied in this paper; that is, the fractional order of the inductor, capacitor, and memristor is maintained

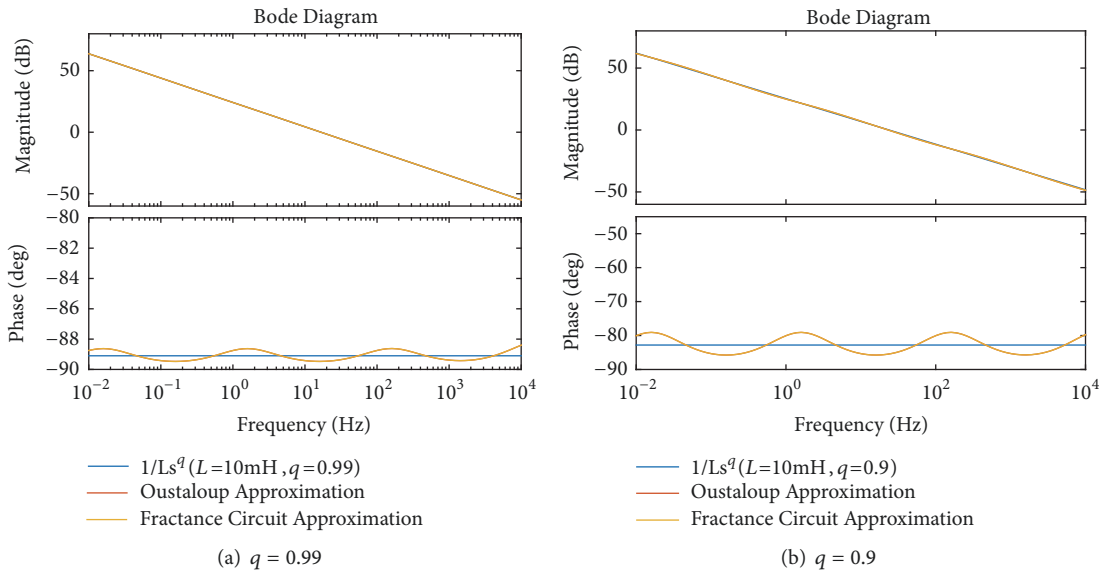

FIGURE 3: The bode diagrams of Oustaloup approximation. (a) $q = 0.99$; (b) $q = 0.9$.

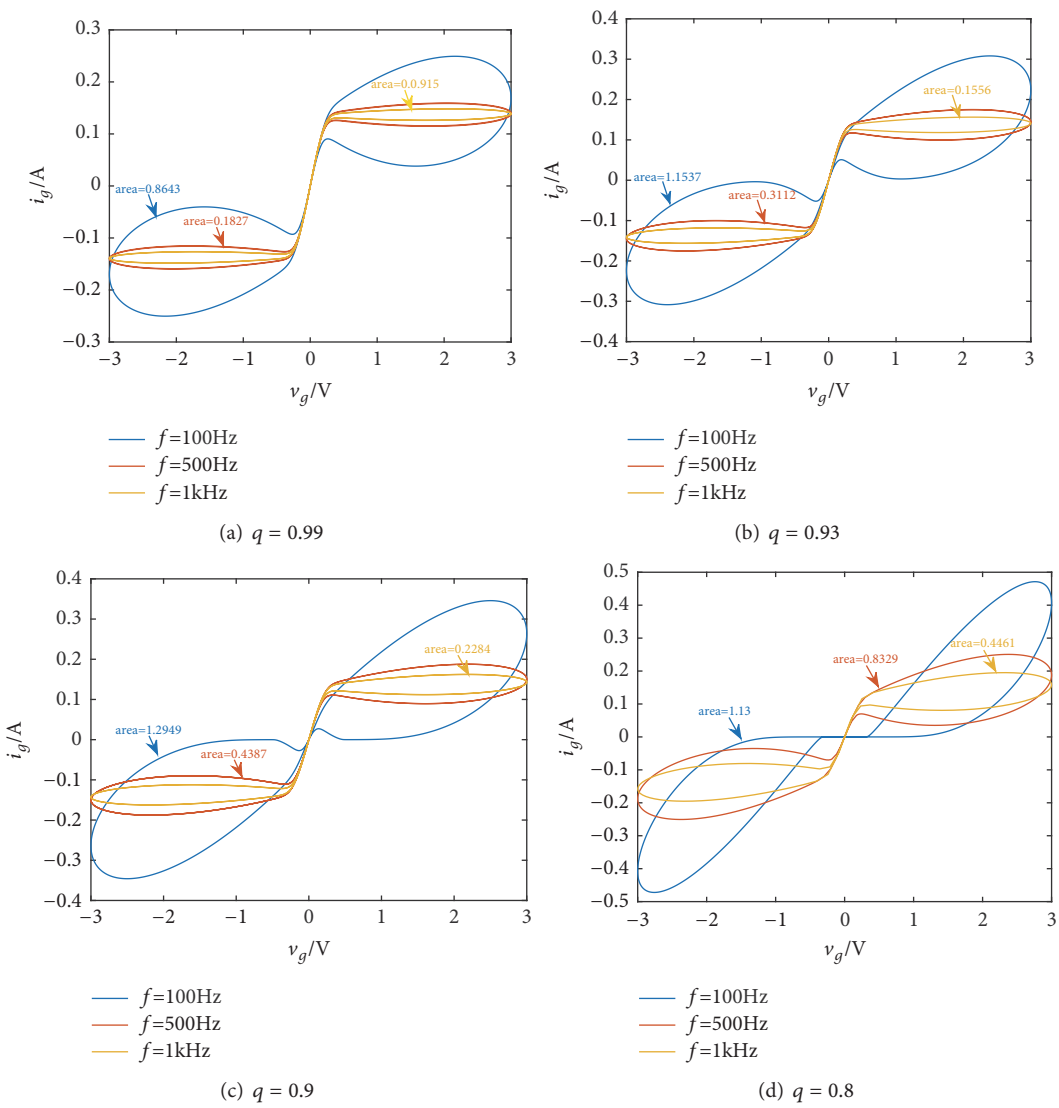

FIGURE 4: The volt-ampere characteristic of FOM with different orders. (a) $q = 0.99$; (b) $q = 0.93$; (c) $q = 0.9$; (d) $q = 0.8$.

Table 2: The inductance parameters of the equivalent chain circuit of the resistor and the fractional-order inductor.

q	R_{in}/Ω	R_1/Ω	R_2/Ω	R_3/Ω	R_4/Ω	R_5/Ω	L_1/H	L_2/H	L_3/H	L_4/H	L_5/H
0.99	891.25	209.451	2.172	0.023	2e(-4)	1e(-7)	0.205	0.212	0.222	0.23	0.011
0.93	446.7	22.6	0.31	0.004	5e(-5)	2e(-7)	0.019	0.026	0.036	0.05	0.019
0.9	316.2	13.7	0.22	0.003	5e(-5)	3e(-7)	0.011	0.012	0.027	0.043	0.025
0.8	100	4.25	0.11	0.0027	6e(-5)	1e(-6)	0.003	0.007	0.017	0.042	0.064

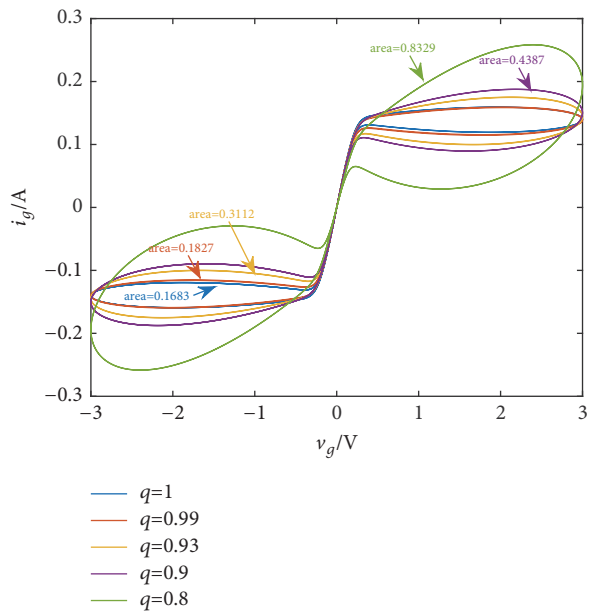

Figure 5: The volt-ampere characteristic with different q when $A = 3$V, $f = 500$Hz.

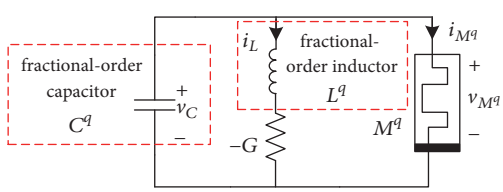

Figure 6: The FOM-based fractional-order chaotic circuit.

as q. When $q = 1$, the system is the integer-order system proposed in [7]. A negative resistor is connected in series by a fractional-order inductor L^q, a fractional-order capacitor C^q and a fractional-order memristor M^q are connected in parallel. v_C represents the voltage of C^q; i_L and i_{M^q} represent the current flowing through $L^q$and M^q, respectively.

Applying the basic circuit law, the following formulas are obtained:

$$C^q \frac{d^q v_C}{dt^q} + i_{M^q} + i_L = 0 \tag{10}$$

$$L^q \frac{d^q i_L}{dt^q} - \frac{i_L}{G} = v_C \tag{11}$$

The mathematical model of FOM is

$$\begin{aligned} i_{M^q} &= \left(i_{L_m} + 2I_S\right) \tanh\left(\rho v_C\right) \\ \frac{d^q i_{L_m}}{dt^q} &= \frac{\left\{\ln\left[2I_S \cosh\left(\rho v_C\right)\right] - \ln\left(i_{L_m} + 2I_S\right)\right\}}{\left(\rho L_m^q\right)} \end{aligned} \tag{12}$$

Then the fractional-order mathematical model of the chaotic circuit is obtained.

$$\begin{aligned} \frac{d^q v_C}{dt^q} &= -\frac{\left[i_L + \left(i_{L_m} + 2I_S\right) \tanh\left(\rho v_C\right)\right]}{C^q} \\ \frac{d^q i_L}{dt^q} &= \frac{\left(v_C + i_L/G\right)}{L^q} \\ \frac{d^q i_{L_m}}{dt^q} &= \frac{\left\{\ln\left[2I_S \cosh\left(\rho v_C\right)\right] - \ln\left(i_{L_m} + 2I_S\right)\right\}}{\left(\rho L_m^q\right)} \end{aligned} \tag{13}$$

Normalize the following variables and circuit parameters:

$$\begin{aligned} v_1 &= \rho v_C, \\ i_1 &= \frac{\rho i_L}{G}, \\ i_m &= \frac{\rho i_{L_m}}{G}, \\ \tau &= \frac{tG}{C^q}, \\ \alpha &= \frac{C^q}{\left(L_m^q G^2\right)}, \\ \beta &= \frac{C^q}{\left(L^q G^2\right)}, \\ \gamma &= \frac{2\rho I_S}{G} \end{aligned} \tag{14}$$

The normalized fractional-order mathematical model of the chaotic circuit is obtained as follows:

$$\begin{aligned} \frac{d^q v_1}{d\tau^q} &= -i_1 - \left(i_m + \gamma\right) \tanh\left(v_1\right) \\ \frac{d^q i_1}{d\tau^q} &= \beta\left(v_1 + i_1\right) \\ \frac{d^q i_m}{d\tau^q} &= \alpha \ln\left[\gamma \cosh\left(v_1\right)\right] - \alpha \ln\left(i_m + \gamma\right) \end{aligned} \tag{15}$$

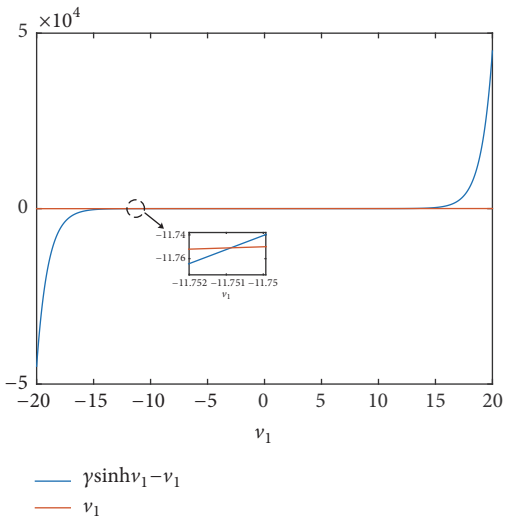

Figure 7: Solution of (19).

When the values of the fractional-order capacitor, inductor, and resistor are set as $C^q = 5\text{nF}$, $L^q = 25\text{mH}$, $G = 0.65\text{mS}$, and $L_m^q = 10\text{mH}$, respectively, values of three parameters can be obtained as

$$\begin{aligned} \alpha &= 1.1834, \\ \beta &= 0.4734, \\ \gamma &= 1.8525 \times 10^{-4} \end{aligned} \tag{16}$$

2.3. Equilibrium Point and Its Stability. Make the left side of (15) equal to zero,

$$\begin{aligned} 0 &= -i_1 - (i_m + \gamma)\tanh(v_1) \\ 0 &= \beta(v_1 + i_1) \\ 0 &= \alpha \ln[\gamma \cosh(v_1)] - \alpha \ln(i_m + \gamma) \end{aligned} \tag{17}$$

The equilibrium point can be obtained as

$$O = [\tilde{v}_1, -\tilde{v}_1, \gamma \cosh(\tilde{v}_1) - \gamma] \tag{18}$$

The value of $\tilde{v}_1$ can be obtained by solving transcendental equations

$$\gamma \sinh(\tilde{v}_1) - \tilde{v}_1 = 0 \tag{19}$$

Equation (19) has a zero solution and a pair of symmetric nonzero solutions, then system (15) has a zero equilibrium point $O_0 = (0, 0, 0)$ and a pair of nonzero equilibrium points $O_{2,3} = (\pm 11.751, \mp 11.751, 11.752)$. Two nonzero equilibrium points are obtained by parameters in (16). As shown in Figure 7, the blue and orange lines represent the trajectory of $x_1 = \gamma \sinh(v_1)$ and $x_2 = v_1$, respectively. The intersection point is the value of v_1.

The Jacobian matrix of the equilibrium point is

$$J = \begin{bmatrix} -\tanh(\tilde{v}_1) & -1 & -\gamma \operatorname{sech}(\tilde{v}_1) \\ 0 & \beta & \beta \\ -\alpha \operatorname{sech}\dfrac{(\tilde{v}_1)}{\gamma} & 0 & \alpha \tanh(\tilde{v}_1) \end{bmatrix} \tag{20}$$

The characteristic equation is

$$O(\lambda) = \det(1\lambda - J) = \lambda^3 + l\lambda^2 + m\lambda + n = 0 \tag{21}$$

where

$$\begin{aligned} l &= (1-\alpha)\tanh(\tilde{v}_1) - \beta \\ m &= (1-\alpha)\beta \tanh(\tilde{v}_1) + \alpha \operatorname{sech}^2(\tilde{v}_1) \\ n &= \alpha\beta\left[\tanh^2(\tilde{v}_1) + \operatorname{sech}^2(\tilde{v}_1) + \operatorname{sech}\frac{(\tilde{v}_1)}{\gamma}\right] \end{aligned} \tag{22}$$

The eigenvalues at three equilibrium points are $O_0 : \lambda_{1,2} = -7.0869 \pm j12.498$, $\lambda_3 = 14.6473$, $O_{1,2} : \lambda_1 = -0.9849$, $\lambda_2 = 1.2125$, $\lambda_3 = 0.4292$. O_0 is an unstable saddle-focus which has one positive root and two complex conjugate roots with negative real parts; $O_{1,2}$ are two unstable node-focuses having two positive roots and one negative root. Therefore, a chaotic orbit can be excited from the unstable saddle-focus O_0 and affected by the two unstable node-focuses $O_{1,2}$, leading to the appearance of double scroll chaotic attractor.

2.4. Characteristic Curve of Chaotic Circuit. The fractional-order mathematical model of the generalized FOM-based chaotic circuit has been derived, then numerical simulations can be realized. The simulation of the fractional-order differential equation (15) can be carried out by Oustaloup approximation method. Circuit parameters are taken as (16). When the order q is 0.99 and initial values are set to be $(0, 0.01, 0)$ and $(0, -0.01, 0)$, respectively, the chaotic trajectories of system (15) is shown in Figure 8.

The phase trajectory with initial value of (0,0.001,0) is plotted with pink lines, and the trajectory with (0,-0.01,0) is plotted with black lines, and the two colors correspond to two initial conditions in subsequent chapters, respectively. As depicted in Figure 8, the chaotic attractor is a double scroll and the fractional-order memristive circuit generates complex attractor topology. Meanwhile, the volt-ampere characteristic curve of the generalized FOM is depicted in Figure 9; the pinched hysteresis loop verifies the validity of the proposed fractional-order generalized memristor. The Poincaré Section of $v_1 - i_m$ when $i_1 = 0$ is depicted in Figure 10, the existence of chaos is verified by regular and closed trajectory.

It should be noted that, in the case of 0.99 order and fixed parameters, the phase trajectory curves of fractional-order circuits under two initial conditions are approximately the same. But with the different order or circuit parameters, the fractional-order circuits will generate more complex dynamic behavior, which will be advanced in the next section.

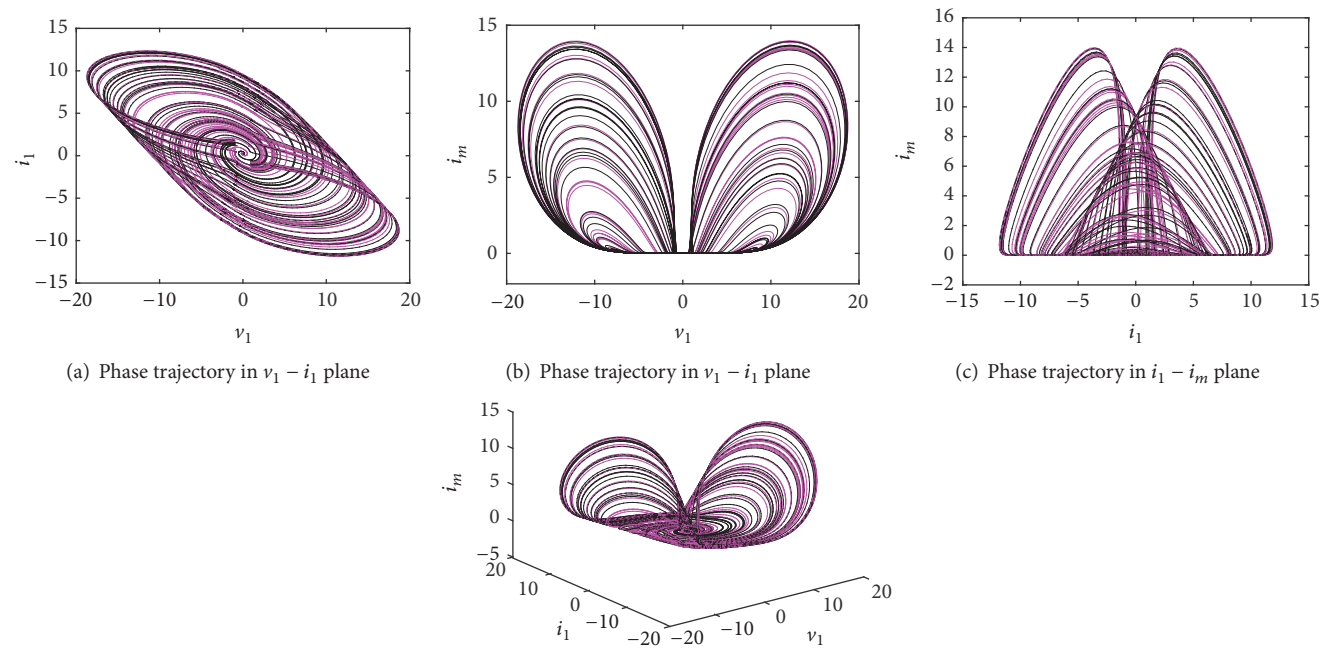

(a) Phase trajectory in $v_1 - i_1$ plane

(b) Phase trajectory in $v_1 - i_1$ plane

(c) Phase trajectory in $i_1 - i_m$ plane

(d) Phase trajectory in $v_1 - i_1 - i_m$ plane

Figure 8: Phase trajectories of fractional-order memristive system at order 0.99; (a) phase trajectory in $v_1 - i_1$ plane; (b) phase trajectory in $v_1 - i_1$ plane; (c) phase trajectory in $i_1 - i_m$ plane; (d) phase trajectory in $v_1 - i_1 - i_m$ plane.

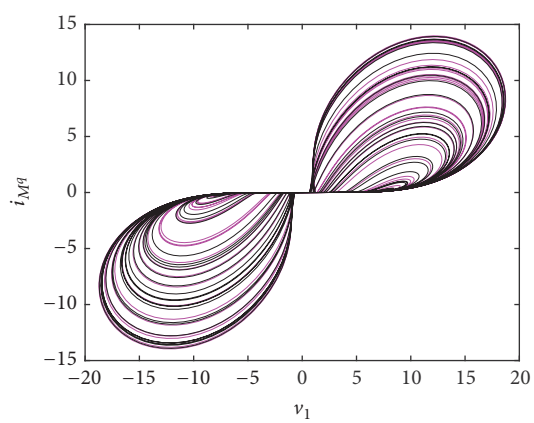

Figure 9: The volt-ampere characteristic curve of the FOM system.

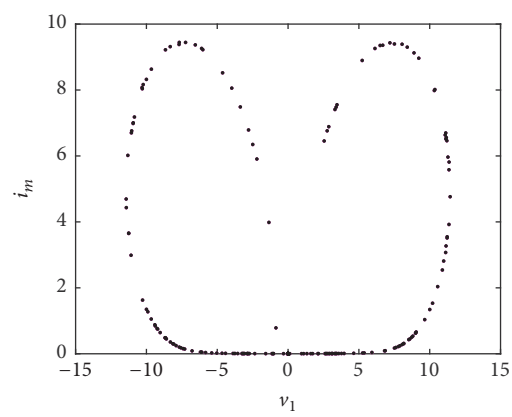

Figure 10: The Poincaré Section of $v_1 - i_m$ when $i_1 = 0$.

3. Dynamic Behavior Analysis of the Fractional-Order Memristor Chaotic System

3.1. The Influence of the Order on the Dynamic Behavior of the System. When the order q varies between regions [0.8, 1], the bifurcation diagram for the variable v_1 versus q is shown in Figure 11.

The coexisting period limit cycle and the spiral chaotic attractor under different initial conditions in the interval of [0.895, 0.947] are a phenomenon worthy of further investigation. For the same initial conditions, the maxima value of the up and down jump variables results in a discontinuity in dynamic behavior. And the dynamic behavior under two initial conditions just happens to form a coexisting period phenomenon. After entering the double scroll chaos, the trajectories are interlaced into the same closed region. The phase trajectory of the system from $q = 0.88$ to $q = 0.962$ is shown in Figure 12. It reveals that the system has experienced a single-period limit cycle, coexisting upper and lower single-period limit cycles, double-period limit cycles, and spiral chaotic attractors, and finally enters the double scroll chaotic attractor. Figure 12(f) shows a multiperiod state occurring in a narrow periodic window at order 0.962. Further, in Figure 12(a), the pink trajectory is covered by the black trajectory, so the pink trajectory is not seen, and the pink and black trajectories are interlaced in Figure 12(f), so that the coexisting phenomenon is not seen. The chaotic phase diagram further confirms that the fractional-order

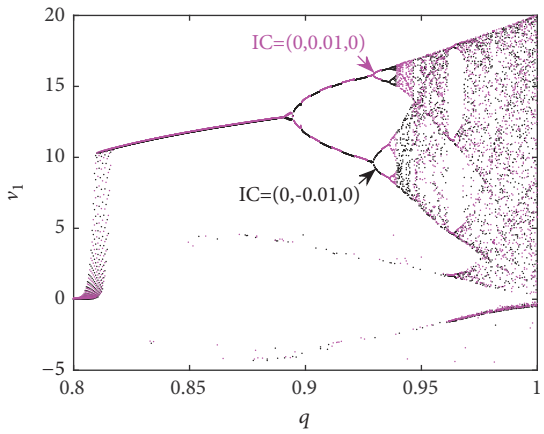

Figure 11: Bifurcation diagrams of the variable v_1 versus q.

chaotic circuit based on the FOM can generate rich dynamic behavior.

3.2. The Influence of System Parameters on System Dynamics Behaviors. When the order is 0.99 and 0.9, the bifurcation diagram of variable v_1 varying with system parameter β is shown in Figure 13. It can be seen that the system moves from the single-period limit cycle to the coexisting upper and lower period limit cycle, then from the coexisting upper and lower four-period limit cycle to the coexisting upper and lower spiral chaotic attractor through period doubling bifurcation, and finally enters the complete chaos. But on the whole, the coexisting bifurcation mode of the system when the order is 0.99 lags behind the one when the order is 0.9.

Comparing with the integer-order system, in the process from single-period limit cycle to period doubling bifurcation, the state of the system is interrupted once when the order is 1, 7 times when the order is 0.99, and 8 times when the order is 0.9, so the frequency of the system state alternating changes increases with the decrease of the order. One can see that the dynamic behavior of the system from single-period limit cycle to chaos via period doubling bifurcation is similar. But in the whole interval, with the decrease of order, the whole behavior has the tendency of backward delay. The system states under typical parameters are compared as shown in Table 3.

Figure 14 reveals that the trajectory of system (15) undergoes coexisting upper and lower single-period limit cycle, coexisting upper and lower double-period limit cycles, coexisting upper and lower four-period limit cycles, coexisting spiral chaotic attractors, multiperiod limit cycles in narrow periodic windows, and complete chaos.

To compare with the case of integer-order system, Figure 15 shows phase diagrams in $v_1 - i_1 - i_m$ space for different β at $q = 1$ and $q = 0.9$, in which the systems are double scroll chaotic states in integer-order system (Figures 15(a) and 15(b)). And the systems are double-period limit cycles at $\beta = 0.6$ (Figure 15(c)) and spiral attractor at $\beta = 0.62$ (Figure 15(d)) in fractional-order system. Figures 14 and 15 are consistent with the bifurcation diagram of Figure 13(b).

3.3. Phenomenon of Antimonotonic Coexisting Bubbles. When the order is 0.99 and α takes different values, the bifurcation diagram of the system variable v_1 varying with the parameter β is shown in Figure 16, in which the variation interval of β is $[0.15, 0.6]$. The phenomenon of antimonotone coexisting bubbles is revealed.

This phenomenon has been found in some nonlinear systems, such as jerk system [28–30] and Chua's circuit [31]. There is an antimonotonic coexisting upper and lower periodic limit cycle bubble at $\alpha = 0.7$, and there is a coexisting upper and lower double-period bubble in the interval $[0.3, 0.5]$ at $\alpha = 0.76$, and there are coexisting upper and lower double-period and four-period bubbles at $\alpha = 0.779$, then the system shows a coexisting upper and lower chaotic band and finally returns to the single-period limit cycle through an antidoubling period bifurcation at $\alpha = 0.8$, and then there are no antimonotonic coexistence bubbles at $\alpha = 0.87$.

4. Circuit Simulation Experiment

In this section, circuit simulations are carried out by Pspice. The fractional-order capacitor and inductor in the FOM-based chaotic circuit are realized by equivalent unit circuits. The equivalent circuit of fractional-order inductor has been introduced in forward part, and the equivalent circuit structure of fractional-order capacitor is shown in Figure 17.

The equivalent circuit expression of the fractional-order capacitor in complex frequency domain is

$$F(s) = \frac{1}{C}s^{-q} = R_{\text{in}} + \sum_{k=1}^{n} \frac{1/C_k}{(s + 1/R_k C_k)} \tag{23}$$

Order q is set as 0.99 and 0.88; L^q, L_m^q, and C^q in Figure 6 are selected as 25mH, 10mH, and 5nF. By Oustaloup approximation technique, the corresponding values of inductance and resistance are calculated in Tables 4 and 5. The bode diagrams of Oustaloup approximation of C^q=5nF and $L^q = 25$mH are shown in Figure 18.

Figure 19 is the circuit structure diagram of simulation in Pspice. The calculated resistance, inductance, and capacitance are used to form equivalent fractional-order inductor and capacitor, respectively. In addition, four diodes 1N4148 and a 1538.5Ω negative resistance which is used to replace conductor of 0.65mS are selected to form fractional-order chaotic circuit in Figure 6.

The phase trajectory at order 0.99 is shown in Figure 20, where the circuit operates in a double scroll chaotic state.

At order 0.88, the circuit presents the limit cycle; the projection on the $v_C - i_L$ and $v_C - i_{L_m}$ plane is shown in Figures 21(a) and 21(b), respectively.

In order to compare with the circuit state of integer-order system, Figures 22(a) and 22(b) are projection on the $v_C - i_L$ and $v_C - i_{L_m}$ plane under the same default initial conditions when $q = 1$. The circuit simulation is in good agreement with the theoretical and numerical analysis. It is proved that the chaotic circuit based on the generalized fractional-order memristor has abundant dynamic behavior.

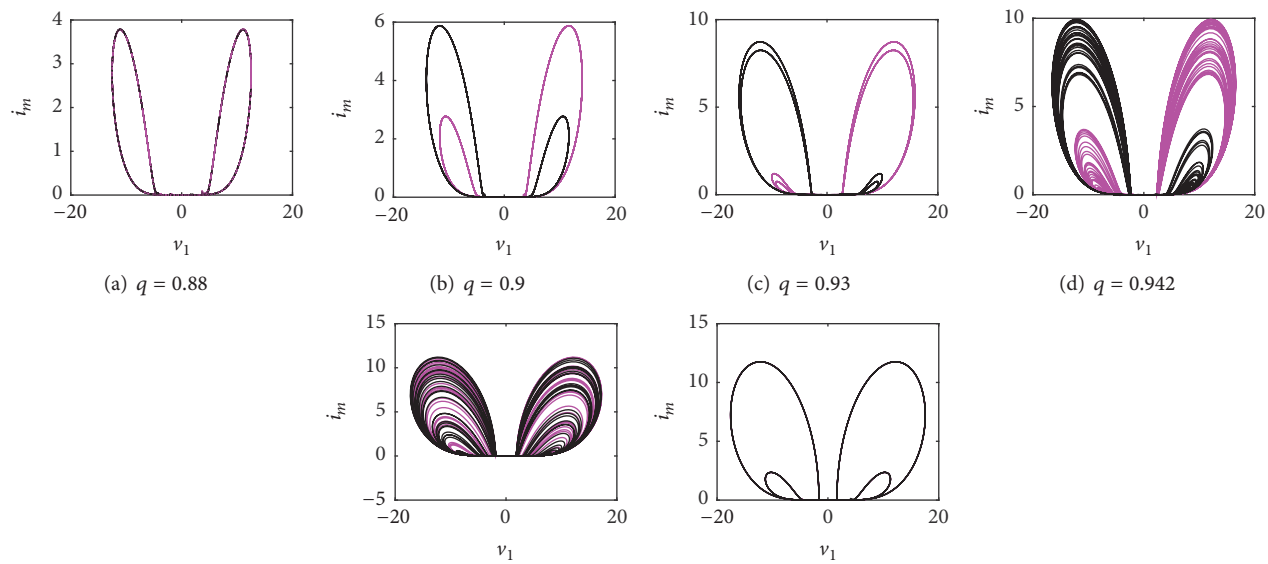

(a) $q = 0.88$ (b) $q = 0.9$ (c) $q = 0.93$ (d) $q = 0.942$

(e) $q = 0.955$ (f) $q = 0.962$

Figure 12: System phase trajectories under different orders; (a) $q = 0.88$; (b) $q = 0.9$; (c) $q = 0.93$; (d) $q = 0.942$; (e) $q = 0.955$; (f) $q = 0.962$.

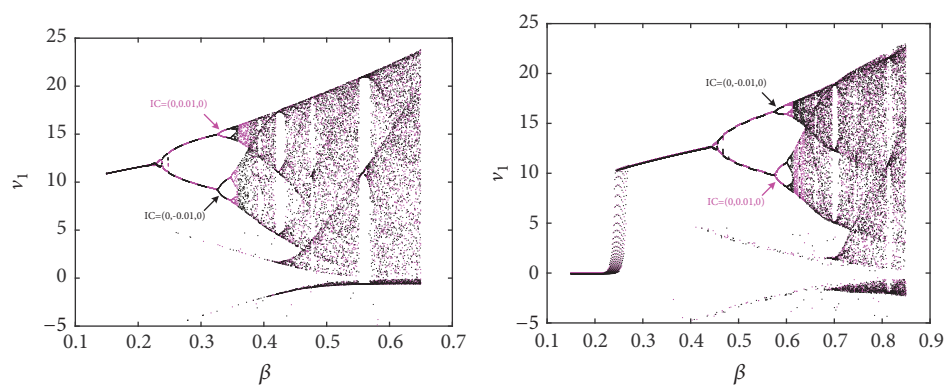

(a) $q = 0.99$ (b) $q = 0.9$

Figure 13: The bifurcation diagrams under different orders; (a) $q = 0.99$; (b)$q = 0.9$.

Table 3: Different system states under different values of β and q.

values of β	orders	system states
$\beta = 0.21$	$q = 1$	coexisting upper and lower period limit cycles
	$q = 0.99$	single limit cycles
	$q = 0.9$	single limit cycles
$\beta = 0.31$	$q = 1$	single scroll spiral chaotic attractor
	$q = 0.99$	coexisting upper and lower period limit cycles
	$q = 0.9$	single limit cycles
$\beta = 0.36$	$q = 1$	multiple period limit cycles
	$q = 0.99$	single scroll spiral chaotic attractor
	$q = 0.9$	single limit cycles
$\beta = 0.56$	$q = 1$	double scroll chaotic attractor
	$q = 0.99$	multiple period limit cycles
	$q = 0.9$	coexisting upper and lower period limit cycles

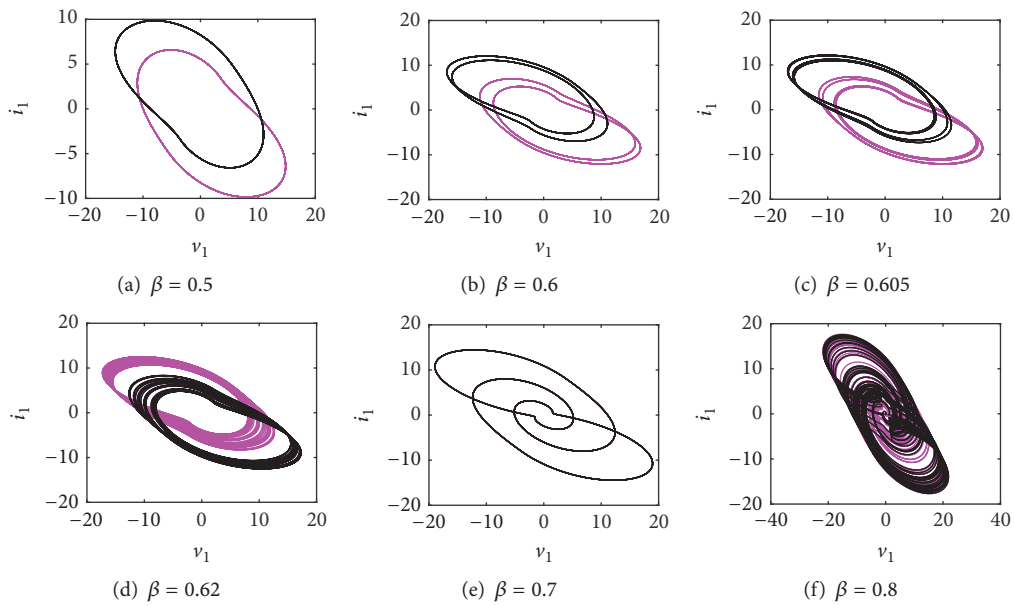

(a) $\beta = 0.5$ (b) $\beta = 0.6$ (c) $\beta = 0.605$

(d) $\beta = 0.62$ (e) $\beta = 0.7$ (f) $\beta = 0.8$

Figure 14: Phase trajectories of the system varying with parameter β at order 0.9; (a) $\beta = 0.5$; (b) $\beta = 0.6$; (c) $\beta = 0.605$; (d) $\beta = 0.62$; (e) $\beta = 0.7$; (f) $\beta = 0.8$.

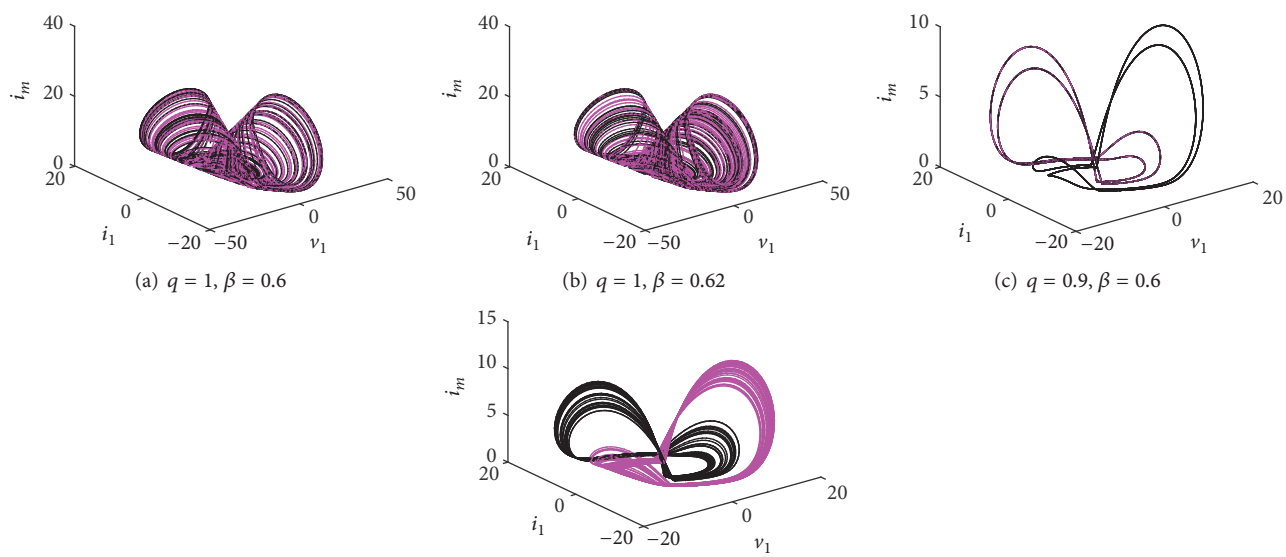

(a) $q = 1, \beta = 0.6$ (b) $q = 1, \beta = 0.62$ (c) $q = 0.9, \beta = 0.6$

(d) $q = 0.9, \beta = 0.62$

Figure 15: Phase trajectories in $v_1 - i_1 - i_m$ space of integer-order and fractional-order memristive system; (a) $q = 1$, $\beta = 0.6$; (b) $q = 1$, $\beta = 0.62$; (c) $q = 0.9$, $\beta = 0.6$; (d) $q = 0.9$, $\beta = 0.62$.

Table 4: The resistance of the equivalent chain circuit of fractional-order inductor and capacitor.

	q	$R_{in}(\Omega)$	$R_1(\Omega)$	$R_2(\Omega)$	$R_3(\Omega)$	$R_4(\Omega)$	$R_5(\Omega)$	$R_6(\Omega)$	$R_7(\Omega)$
L^q (25mH)	0.99	1.81e5	2.28e4	247.51	2.71	0.03	3.3e-4	1.6e-7	0.04
	0.88	1.21e5	8.04e3	97.9	1.2	0.015	1.8e-4	2.1e-7	0.062
L_m^q (10mH)	0.99	7.2e4	9.1e4	99	1.1	0.012	1.3e-4	6.4e-8	0.015
	0.88	4.8e4	3.2e3	39.2	0.48	0.006	7.3e-5	8.5e-8	0.025
C^q (5nF)	0.99	27.6	219.3	2e4	1.8e6	1.7e8	1.5e10	3.1e13	1.3e8
	0.88	41.3	622	5e4	4.2e6	3.4e8	2.7e10	2.4e13	8e7

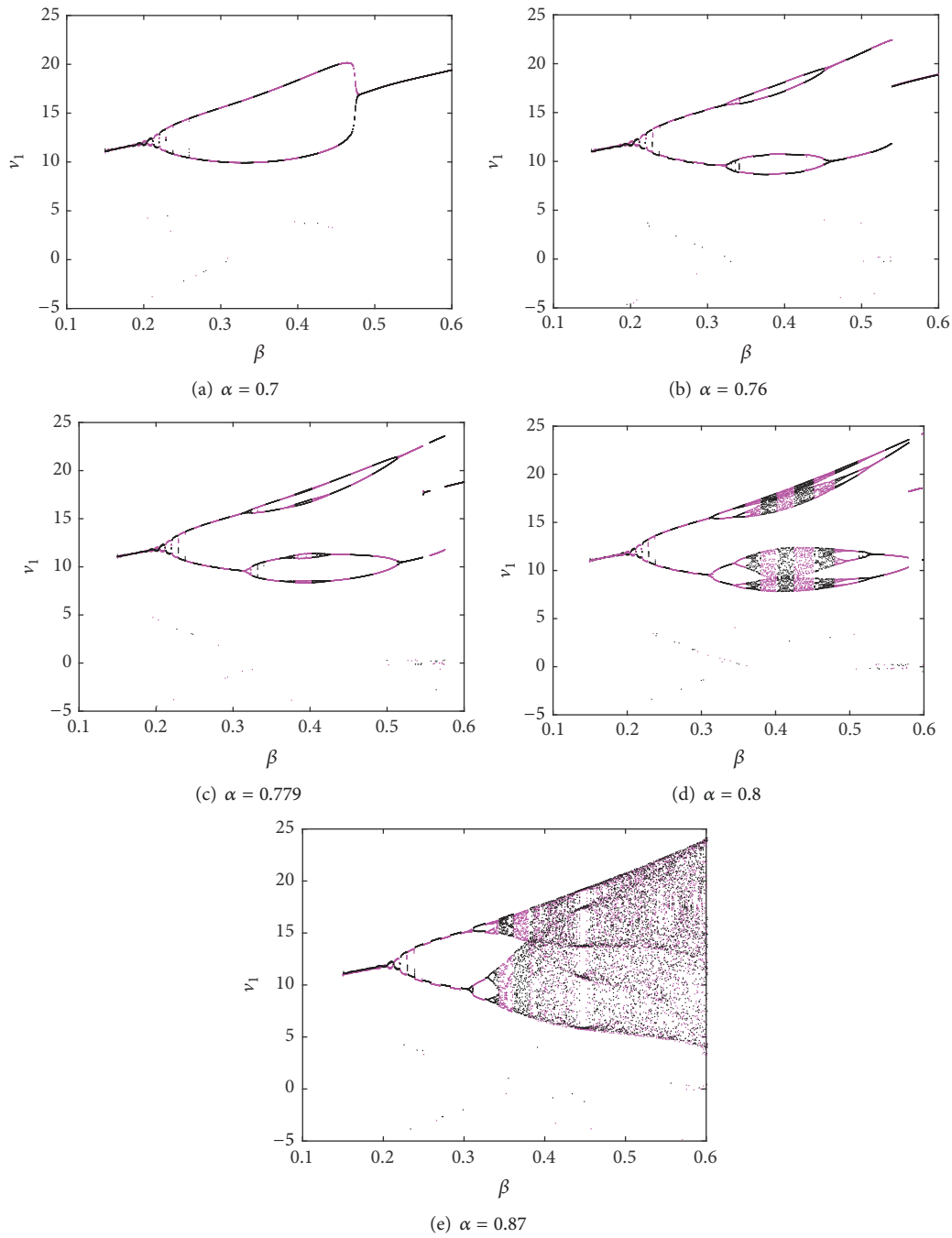

FIGURE 16: Antimonotonic coexisting bubble phenomenon at order 0.99 with different α; (a) $\alpha = 0.7$; (b) $\alpha = 0.76$; (c) $\alpha = 0.779$; (d) $\alpha = 0.8$; (e) $\alpha = 0.87$.

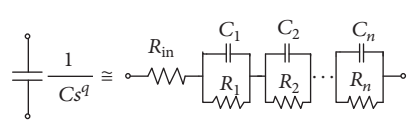

FIGURE 17: Equivalent circuit of fractional-order capacitor.

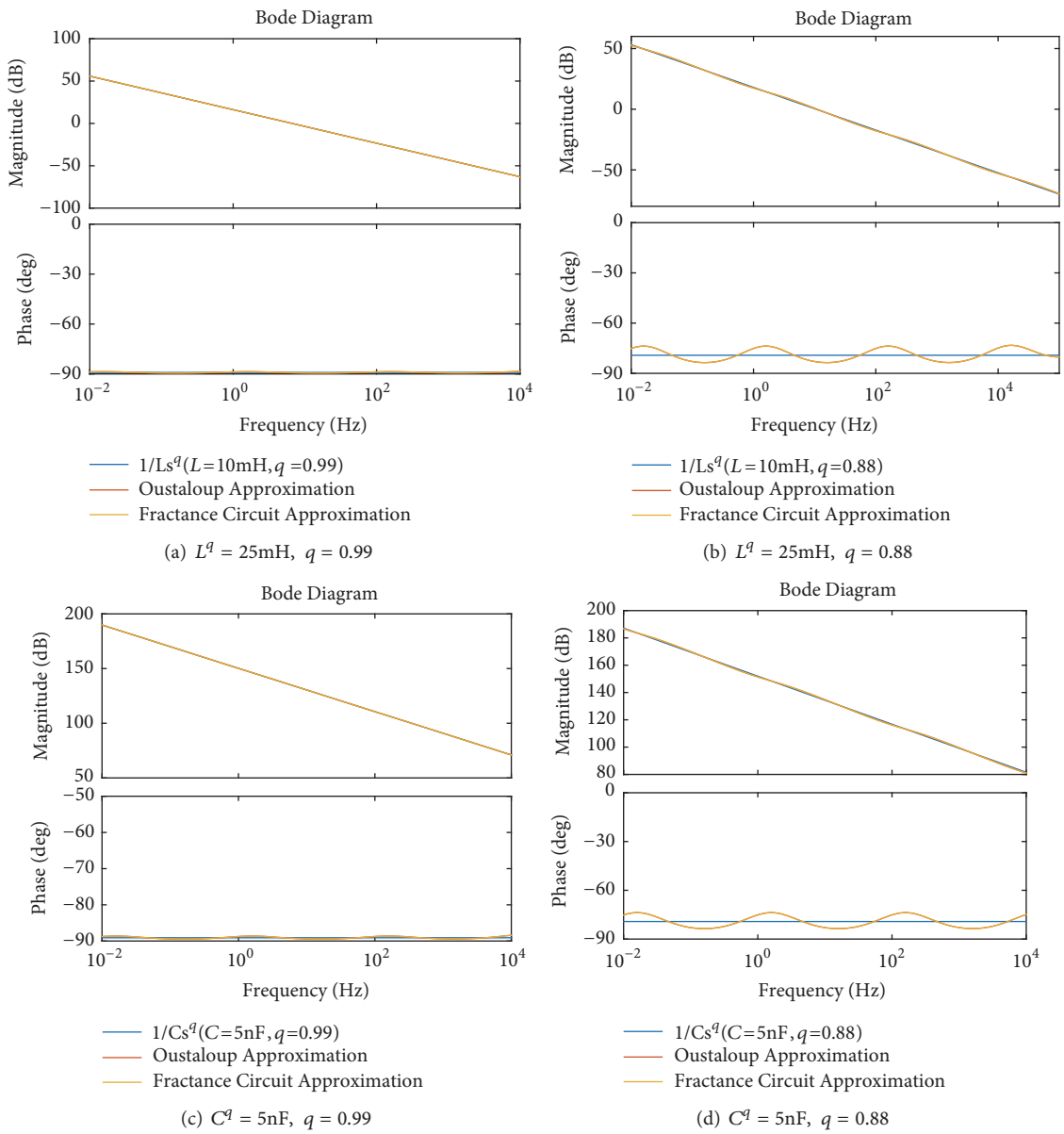

Figure 18: The bode diagrams of Oustaloup approximation of C^q. (a) $L^q = 25\text{mH}, q = 0.99$; (b) $L^q = 25\text{mH}, q = 0.88$; (c) $C^q = 5\text{nF}, q = 0.99$; (d) $C^q = 5\text{nF}, q = 0.88$.

Table 5: The parameters of the equivalent chain circuit of fractional-order inductor and capacitor.

	q	L_1(H)	L_2(H)	L_3(H)	L_4(H)	L_5(H)	L_6(H)	L_7(H)
L^q (25mH)	0.99	0.218	0.236	0.26	0.28	0.312	0.03	7.1e3
	0.88	0.073	0.088	0.11	0.135	0.164	0.038	1.1e4
L_m^q (10mH)	0.99	0.09	0.09	0.1	0.11	0.125	0.012	2.8e3
	0.88	0.03	0.035	0.043	0.054	0.066	0.015	4.4e3
	q	C_1(F)	C_2(F)	C_3(F)	C_4(F)	C_5(F)	C_6(F)	C_7(F)
C^q (5nF)	0.99	4.3e-8	4.7e-8	5.2e-8	5.7e-8	6.2e-8	6e-9	0.0014
	0.88	1.4e-8	1.8e-8	2.2e-8	2.7e-8	3.3e-8	7.6e-9	0.002

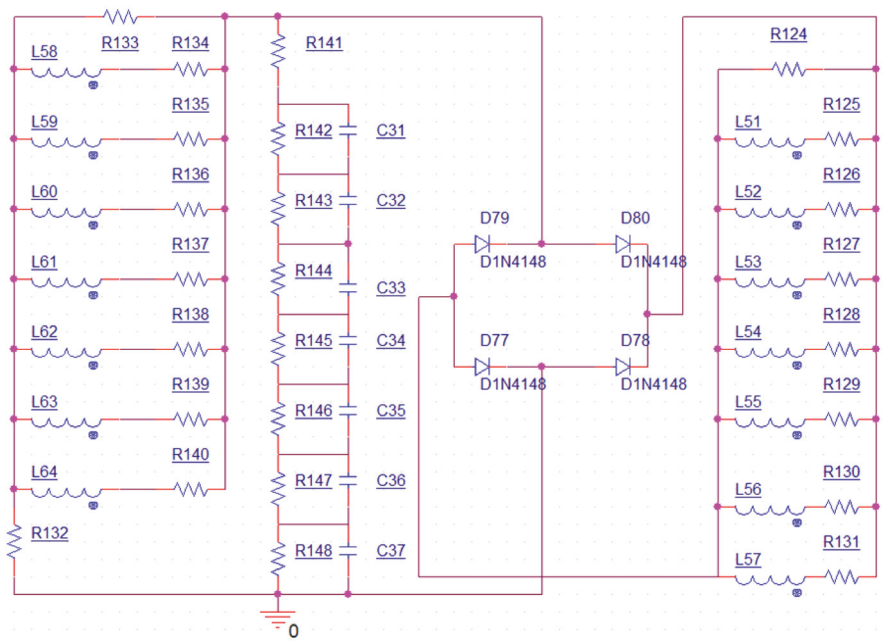

FIGURE 19: Circuit structure diagram Pspice simulation.

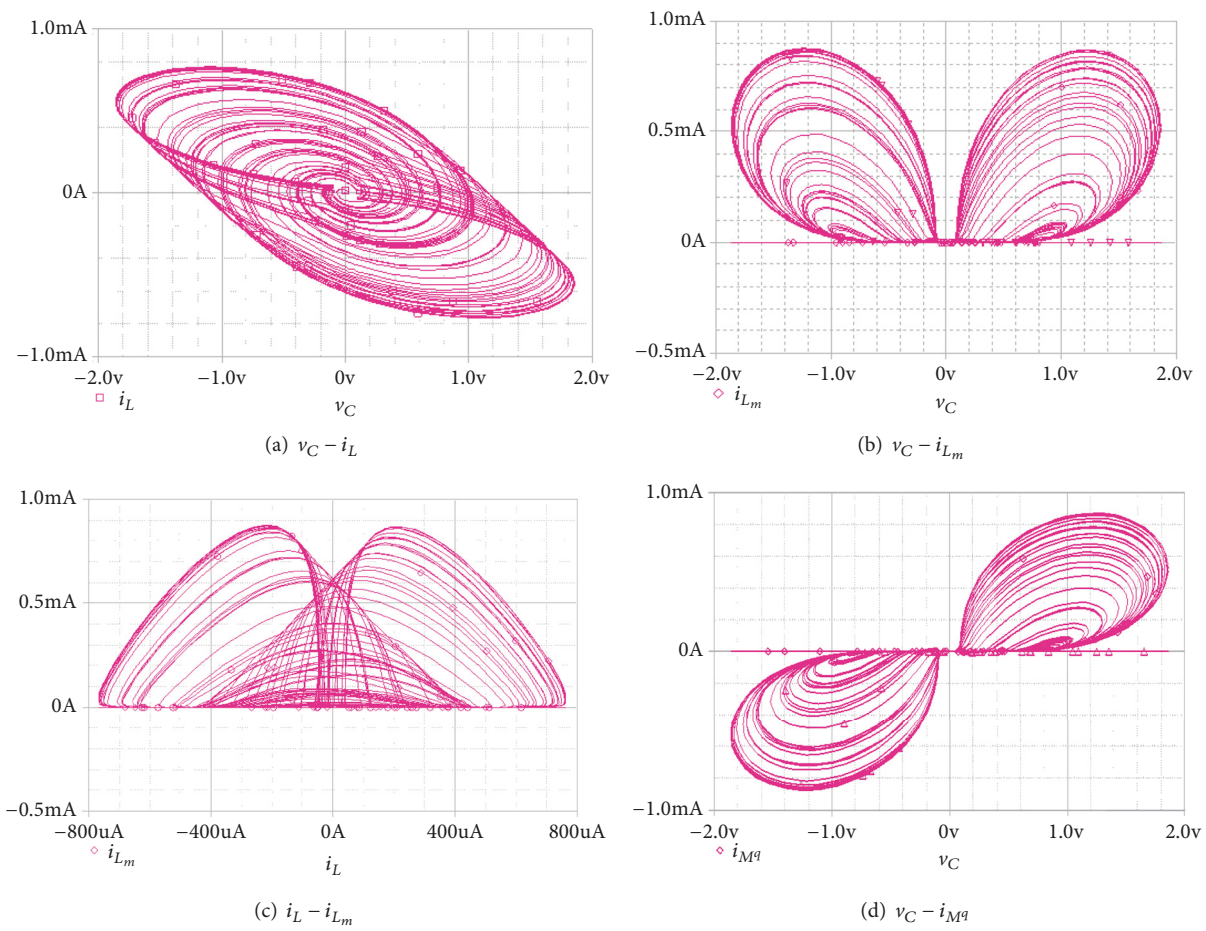

FIGURE 20: Phase trajectories of variable of fractional-order memristive circuits when $q = 0.99$; (a) projection on the $v_C - i_L$ plane; (b) projection on the $v_C - i_{L_m}$ plane; (c) projection on the $i_L - i_{L_m}$ plane; (d) projection on the $v_C - i_{M^q}$ plane.

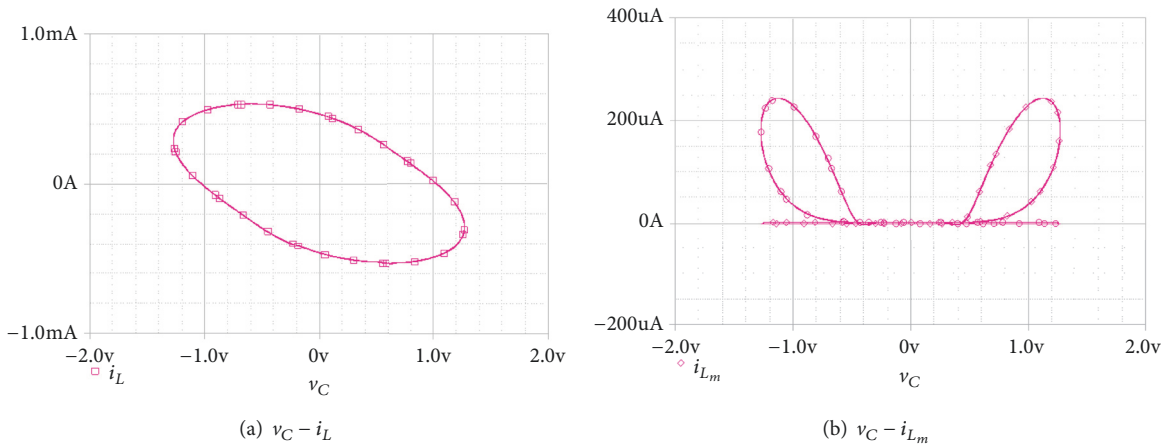

Figure 21: Phase trajectories of variable of fractional-order and integer-order memristive circuits; (a) projection on the $v_C - i_L$ plane when $q = 0.88$; (b) projection on the $v_C - i_{L_m}$ plane when $q = 0.88$.

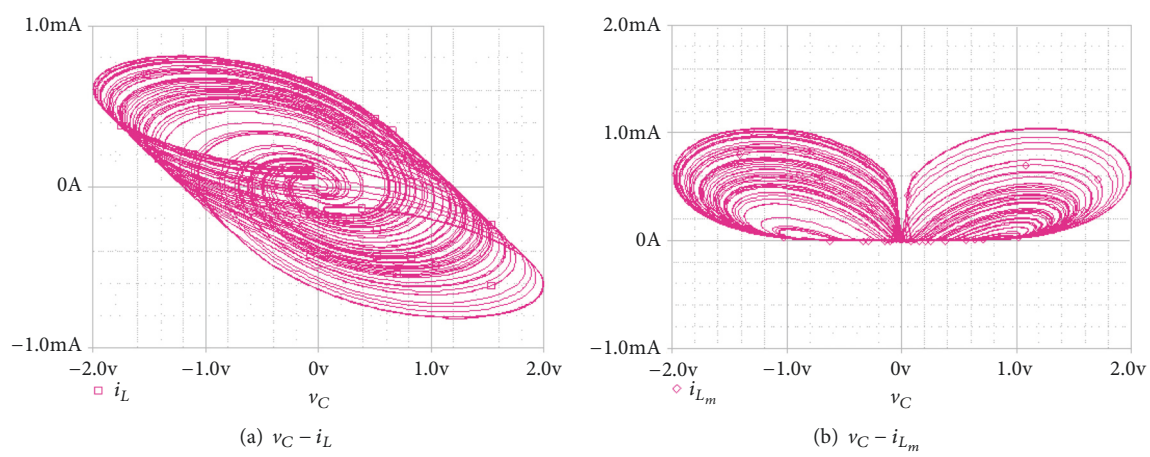

Figure 22: Phase trajectories of variable of fractional-order and integer-order memristive circuits; (a) projection on the $v_C - i_L$ plane when $q = 1$; (b) projection on the $v_C - i_{L_m}$ plane when $q = 1$.

5. Conclusion

A generalized fractional-order memristor based on fractional-order inductor and diode bridge is proposed and its memristive characteristics are verified. Then a fractional-order chaotic circuit composed of a fractional-order capacitor, inductor, and a negative resistor is proposed. It has an unstable saddle-focus and two unstable node-focuses, which indicates that the system is a double scroll chaotic system with fixed parameters. Then the bifurcation diagram of the system changing with the order is studied. Combining with the system trajectory, under different initial conditions, the system will experience single-period limit cycles, coexisting upper and lower single-period limit cycle, multiple-period limit cycles, and spiral chaos, and finally enters into double scroll chaotic state when the order is less than 1. Then the bifurcation diagrams of the system with one of the parameters at different orders are studied. It presents that the dynamic behavior with same fixed system parameters at different orders is similar to delay process. At the same time, it is found that the fractional-order system has antimonotonic behavior consisting of forward and antiperiodic coexisting upper and lower periodic or chaotic band states. Finally, the chaotic circuit composed of equivalent fractional-order inductor and capacitor is simulated to verify the abundant dynamic behavior of memristive circuit. Compared with other fractional-order memristive chaotic circuits, the chaotic system based on fractional-order memristor has a simpler topology but has abundant dynamic behavior.

Data Availability

The data used to support the findings of this study are available from the corresponding author upon request.

Conflicts of Interest

The authors declare that there are no conflicts of interest regarding the publication of this paper.

Acknowledgments

This work was supported by the National Natural Science Foundation of China (Grant no. 51507134), Scientific Research Program Funded by Shaanxi Provincial Department of Water Resources (Grant no. 2017slkj-15), Natural Science Foundation of Shaanxi Province (Grant no. 2018JM5068), Key Project of Natural Science Basic Research Plan in Shaanxi Province of China (Grant no. 2018ZDXM-GY-169), and Xi'an Science and Technology Innovation Project (Grant no. 201805037(21)).

References

[1] L. O. Chua, "Memristor—the missing circuit element," *IEEE Transactions on Circuit Theory*, vol. 18, no. 5, pp. 507–519, 1971.

[2] D. B. Strukov, G. S. Snider, D. R. Stewart, and R. S. Williams, "The missing memristor found," *Nature*, vol. 453, pp. 80–83, 2008.

[3] F. Corinto and A. Ascoli, "Memristive diode bridge with LCR filter," *IEEE Electronics Letters*, vol. 48, no. 14, pp. 824-825, 2012.

[4] B. C. Bao, J. J. Yu, F. W. Hu, and Z. Liu, "Generalized memristor consisting of diode bridge with first order parallel RC filter," *International Journal of Bifurcation and Chaos*, vol. 24, no. 11, Article ID 1450143, 2014.

[5] H.-G. Wu, B.-C. Bao, and Q. Xu, "First order generalized memristor emulator based on diode bridge and series RL filter," *Acta Electronica Sinica*, vol. 43, no. 10, pp. 2129–2132, 2015.

[6] B.-C. Bao, P. Wu, H. Bao, M. Chen, and Q. Xu, "Chaotic bursting in memristive diode bridge-coupled Sallen-Key lowpass filter," *IEEE Electronics Letters*, vol. 53, no. 16, pp. 1104-1105, 2017.

[7] B. Bao, L. Xu, N. Wang, H. Bao, Q. Xu, and M. Chen, "Third-order RLCM-four-elements-based chaotic circuit and its coexisting bubbles," *AEÜ - International Journal of Electronics and Communications*, vol. 94, pp. 26–35, 2018.

[8] B. C. Bao, P. Y. Wu, H. Bao, H. G. Wu, X. Zhang, and M. Chen, "Symmetric periodic bursting behavior and bifurcation mechanism in a third-order memristive diode bridge-based oscillator," *Chaos, Solitons & Fractals*, vol. 109, pp. 146–153, 2018.

[9] B. C. Bao, P. Y. Wu, H. Bao, Q. Xu, and M. Chen, "Numerical and experimental confirmations of quasi-periodic behavior and chaotic bursting in third-order autonomous memristive oscillator," *Chaos, Solitons & Fractals*, vol. 106, pp. 161–170, 2018.

[10] S. P. Adhikari, C. Yang, H. Kim, and L. O. Chua, "Memristor bridge synapse-based neural network and its learning," *IEEE Transactions on Neural Networks and Learning Systems*, vol. 23, no. 9, pp. 1426–1435, 2012.

[11] M. Itoh and L. O. Chua, "Memristor cellular automata and memristor discrete-time cellular neural networks," *International Journal of Bifurcation and Chaos*, vol. 19, no. 11, pp. 3605–3656, 2009.

[12] S. P. Adhikari, M. P. Sah, H. Kim, and L. O. Chua, "Three fingerprints of memristor," *IEEE Transactions on Circuit Theory*, vol. 60, no. 11, pp. 3008–3021, 2013.

[13] N. Yang, C. Xu, C. Wu, R. Jia, and C. Liu, "Modeling and analysis of a fractional-order generalized memristor-based chaotic system and circuit implementation," *International Journal of Bifurcation and Chaos*, vol. 27, no. 13, Article ID 1750199, 2017.

[14] Q. Yang, D. Chen, T. Zhao, and Y. Chen, "Fractional calculus in image processing: a review," *Fractional Calculus and Applied Analysis*, vol. 19, no. 5, pp. 1222–1249, 2016.

[15] G.-C. Wu, D. Baleanu, and Z.-X. Lin, "Image encryption technique based on fractional chaotic time series," *Journal of Vibration and Control*, vol. 22, no. 8, pp. 2092–2099, 2016.

[16] N. Yang, Y. Han, C. Wu, R. Jia, and C. Liu, "Dynamic analysis and fractional-order adaptive sliding mode control for a novel fractional-order ferroresonance system," *Chinese Physics B*, vol. 26, no. 8, p. 080503, 2017.

[17] I. Petráš, Y. Q. Chen, and C. Coopmans, "Fractional-order memristive systems," in *Proceedings of the IEEE Conference on Emerging Technologies & Factory Automation*, 2009.

[18] I. Petráš, "Fractional-order memristor-based Chua's circuit," *IEEE Transactions on Circuits System-II: Express Briefs*, vol. 57, no. 12, pp. 975–979, 2010.

[19] D. Cafagna and G. Grassi, "On the simplest fractional-order memristor-based chaotic system," *Nonlinear Dynamics*, vol. 70, no. 2, pp. 1185–1197, 2012.

[20] C. Wu, G. Si, Y. Zhang, and N. Yang, "The fractional-order state-space averaging modeling of the Buck Boost DC/DC converter in discontinuous conduction mode and the performance analysis," *Nonlinear Dynamics*, vol. 79, no. 1, pp. 689–703, 2015.

[21] H. Xi, Y. Li, and X. Huang, "Generation and nonlinear dynamical analyses of fractional-order memristor-based Lorenz systems," *Entropy*, vol. 16, no. 12, pp. 6240–6253, 2014.

[22] L. O. Chua, "Resistance switching memories are memristor," *Applied Physics A-materials Science & Processing*, vol. 102, no. 4, pp. 765–783, 2011.

[23] I. Podlubny, *Fractional Differential Equations: An Introduction to Fractional Derivatives, Fractional Differen-tial Equations, to Methods of Their Solution and Some of Their Applications*, Academic Press, San Diego, Calif, USA, 1998.

[24] O. P. Agrawal, "A general formulation and solution scheme for fractional optimal control problems," *Nonlinear Dynamics*, vol. 38, pp. 323–337, 2004.

[25] J. Chen, Z. Zeng, and P. Jiang, "Global Mittag-Leffler stability and synchronization of memristor-based fractional-order neural networks," *Neural Networks*, vol. 51, pp. 1–8, 2014.

[26] K. Rajagopal, A. Karthikeyan, and A. Srinivasan, "Dynamical analysis and FPGA implementation of a chaotic oscillator with fractional-order memristor components," *Nonlinear Dynamics*, vol. 91, no. 3, pp. 1491–1512, 2018.

[27] L. Teng, H. H. C. Iu, X. Wang, and K. Wang, "Chaotic behavior in fractional-order memristor-based simplest chaotic circuit using fourth degree polynomial," *Nonlinear Dynamics*, vol. 77, no. 1-2, pp. 231–241, 2014.

[28] Z. T. Njitacke, J. kengne, and L. Kamdjeu Kengne, "Antimonotonicity, chaos and multiple coexisting attractors in a simple hybrid diode-based jerk circuit," *Chaos, Solitons & Fractals*, vol. 105, pp. 77–91, 2017.

[29] J. Kengne, A. N. Negou, and D. Tchiotsop, "Antimonotonicity: Chaos and multiple attractors in a novel autonomous memristor-based jerk circuit," *Nonlinear Dynamics*, vol. 88, pp. 2589–2608, 2017.

[30] J. Kengne, A. Nguomkam Negou, and Z. T. Njitacke, "Antimonotonicity, chaos and multiple attractors in a novel autonomous jerk circuit," *International Journal of Bifurcation and Chaos*, vol. 27, Article ID 1750100, 2017.

[31] L. Kocarev, K. Halle, K. Eckert, and L. O. Chua, "Experimental observation of antimonotonicity in Chua's circuit," *International Jouanal of Bifurcation and Chaos*, vol. 3, pp. 1051–1055, 1993.